

Impact of an obstacle on granular flow through apertures

Deepak Sharma^{1,*} and Ashish Bhateja^{1,**}

¹School of Mechanical Sciences, Indian Institute of Technology Goa, Ponda 403401, Goa, India

Abstract. It is not uncommon to observe the flow of discrete entities through narrow openings. Examples include transporting granular media through outlets in hoppers. Developing a robust mechanism to regulate granular flow through apertures without clogging is a central point of various studies conducted over decades. Previous works report that placing an obstacle just above the outlet reduces jamming and improves the flow rate. However, a comprehensive understanding of the dynamics of granular flow in these scenarios remains elusive. In this study, we examine the influence of an obstacle on granular kinematics in a quasi-two-dimensional silo using discrete element computations. The aperture size is large enough to ensure a continuous flow. We vary the frictional characteristics of the walls along the thickness, keeping them either smooth or rough. The vertical placement of the obstacle at which the flow rate becomes equal to the no-obstacle scenario depends on the frictional nature of the walls. In light of this, we show that the velocity and density fields at the exit exhibit contrasting behaviour.

1 Introduction

Granular materials commonly pass through apertures when transported from storage devices such as bins and hoppers in various industrial set-ups [1]. It is not desirable to have grains jammed at the outlet. Accordingly, several ideas have been proposed to obtain a continuous flow. Placing an obstacle right above the exit is one of them [2, 3].

Studies report the influence of the vertical placement of obstacle and/or its size on clogging probability [2–4], and enhancing the flow rate [5, 6]. The large inserts are shown to be better at reducing clogging [3, 4]. In addition, the effect of obstacle shape also has an appreciable impact on clogging at the exit [7]. There is no unified mechanism available governing granular flow through apertures when an obstacle is present [4, 8–10].

In this work, we look at how the frictional characteristics of the walls influence granular flow in the presence of an obstacle. We, however, consider a scenario where no clogging occurs, envisaging that granular mechanics in such a situation would help understand its counterpart with a likelihood of jamming occurrences. This work examines the outflow rate, and the velocity and density fields at the exit utilizing discrete element computations, which are discussed next.

2 Methodology

We computationally investigate a gravity-driven granular flow through an aperture in a quasi-two-dimensional rectangular silo, with a cylindrical obstacle of circular cross-section placed right above the exit, as displayed in Fig. 1.

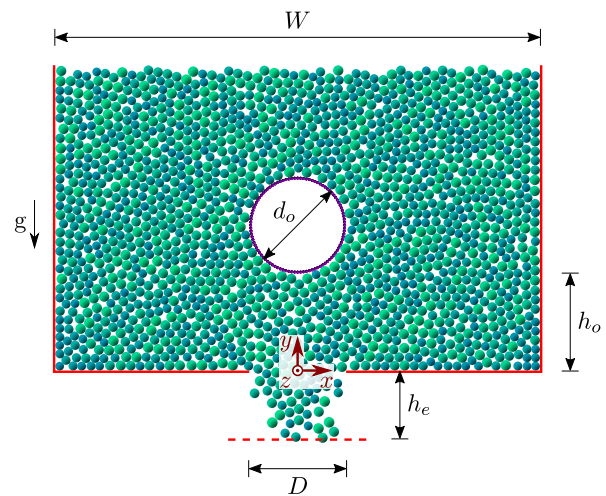


Figure 1. (Front view) Granular flow under gravity in the presence of an obstacle in a quasi-two-dimensional silo. The coordinate axes and geometrical parameters are suitably indicated.

The obstacle and aperture are located symmetrically about the center of the base. The grains are considered dry and non-cohesive spheres, having a size polydispersity of $\pm 10\%$ with mean diameter d . The aperture (D) and obstacle (d_o) sizes are equal and fixed at $D=d_o=10d$. The vertical placement h_o of the obstacle, measured from the outlet, is varied between $5d$ and $25d$; see Fig. 1. The obstacle has a bumpy surface and comprises grains of size $0.3d$. The obstacle axis aligns with the z direction. The thickness and width of the silo are $t = 1.2d$ and $W = 50d$, respectively. The initial fill height of grains is $H \approx 350d$. Periodic boundary conditions are applied along the y di-

*e-mail: deepak20263202@iitgoa.ac.in

**e-mail: ashish@iitgoa.ac.in

rection; grains crossing the vertical location $h_o = 7d$ below the outlet re-enter the system from the top with the same velocity. In doing so, the fill height of grains is largely maintained at its initial value.

The computations are performed employing the discrete element method [11], using an open-source package LAMMPS [12]. A linear spring-dashpot force model is utilized to model grain-grain and grain-wall interactions [13]. The contact force between grains i and j having masses m_i and m_j , respectively, may be resolved into two components: the normal force \mathbf{F}_n and the tangential force \mathbf{F}_t , which are given by

$$\mathbf{F}_n = k_n \delta_n \hat{\mathbf{n}} - m_e \gamma_n \mathbf{v}_n, \quad (1)$$

$$\mathbf{F}_t = -k_t \delta_t - m_e \gamma_t \mathbf{v}_t, \quad (2)$$

where $m_e = m_i m_j / (m_i + m_j)$ is the effective mass, and k and γ represent the spring stiffness and damping coefficient, respectively, with the subscripts ‘ n ’ and ‘ t ’ denoting the normal and tangential directions. The overlap between the touching grains is given by $\delta_n = [0.5(d_i + d_j) - r_{ij}]$, where r_{ij} is the distance between their centres. The unit vector $\hat{\mathbf{n}}$ characterizes the normal direction that goes along the line joining the centres of the contacting grains. The velocities \mathbf{v}_n and \mathbf{v}_t are the normal and tangential components of the relative velocity of grains at the point of contact, and δ_t is the displacement vector in the tangential direction. The magnitude of the tangential force $|\mathbf{F}_t|$ is bounded by the Coulomb frictional force $\mu|\mathbf{F}_n|$, i.e., $|\mathbf{F}_t| \leq \mu|\mathbf{F}_n|$, where μ is the friction coefficient. The quantities of interest presented here are scaled with d , the grain density ρ , and the gravitational acceleration g being the characteristic parameters. The spring stiffness and damping coefficient for normal interactions are $k_n = 10^6$ and $\gamma_n = 200$, respectively. The tangential spring stiffness k_t is $2/7$ times k_n ; the tangential damping coefficient is $\gamma_t = \gamma_n$. The friction coefficient for all interactions is $\mu = 0.4$, and the integration time step is $\Delta t = 10^{-4}$.

3 Results and discussion

Here, we consider two systems in which the front and rear walls, along the z direction (see Fig. 1), are made *smooth* or *rough*. That is, the interaction between grains and front/rear walls is frictionless or frictional, respectively. The number of grains considered for the smooth- and rough-wall systems is 18860 and 18560, respectively. The data reported here are averaged in the steady state over a hundred thousand frames, sampled in ten sets comprising ten thousand snapshots each. A coarse-graining technique is utilized for averaging, taking a Heaviside step function into account. The coarse-grained width is equal to mean diameter d .

3.1 Flow rate

We begin by exploring the mass flow rate variation by changing the vertical placement h_o of the obstacle for the smooth and rough systems. The flow rates are also computed without considering an obstacle for each system,

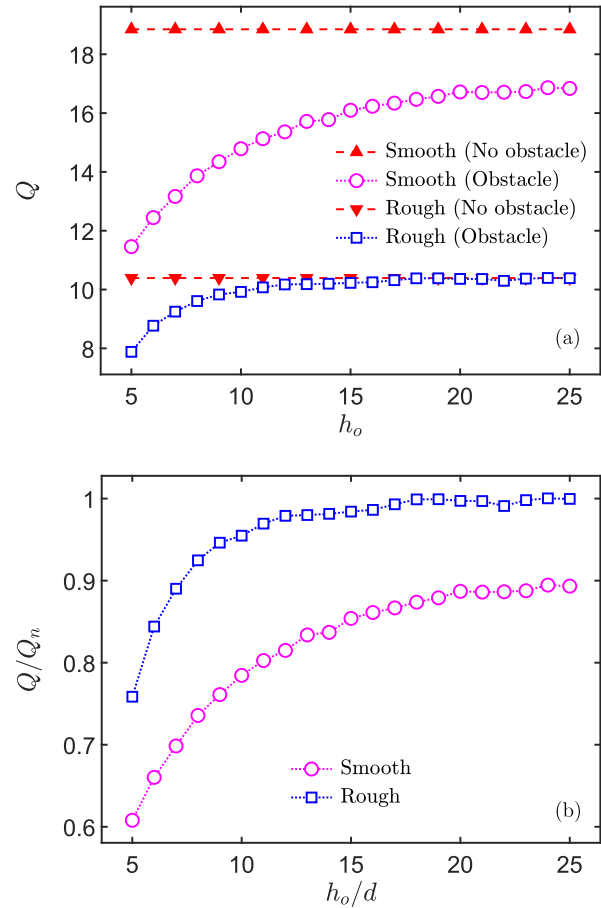


Figure 2. (a) Variation of the mass flow rate Q with the vertical placement h_o of the obstacle. (b) Change in the scaled mass flow rate as h_o varies, with Q_n representing the flow rate without obstacle.

which is taken as a reference for comparison respectively. Figure 2(a) shows the variation of the mass flow rate Q with h_o . We first look at the rough-wall case. As expected, the flow rate is lower due to increased dissipation. Further, the flow rate grows as the obstacle moves vertically away from the exit and attains a nearly constant value, which corresponds to the flow rate without obstacle. We note a similar trend exhibited by Q as h_o increases for the smooth-wall system. However, in contrast to its ‘rough’ counterpart, the flow rate does not reach the reference value for the corresponding no-obstacle case for the vertical placements considered here. The flow rate decreases by nearly 10% for the highest obstacle location for the smooth-wall system.

To appreciate and compare the effect of an obstacle on the flow rates in both systems, they are scaled by their respective values in the absence of an obstacle and are presented in Fig. 2(b). For the closest placement of the obstacle ($h_o = 5d$), it is interesting to note that the reduction in the flow rate by placing an obstacle is less for rough walls. Also, the rate at which the flow rate attains its no-obstacle value is higher for the rough-wall system as h_o varies. Given the seemingly differing behaviours of the smooth and rough systems, it is pertinent to analyse the

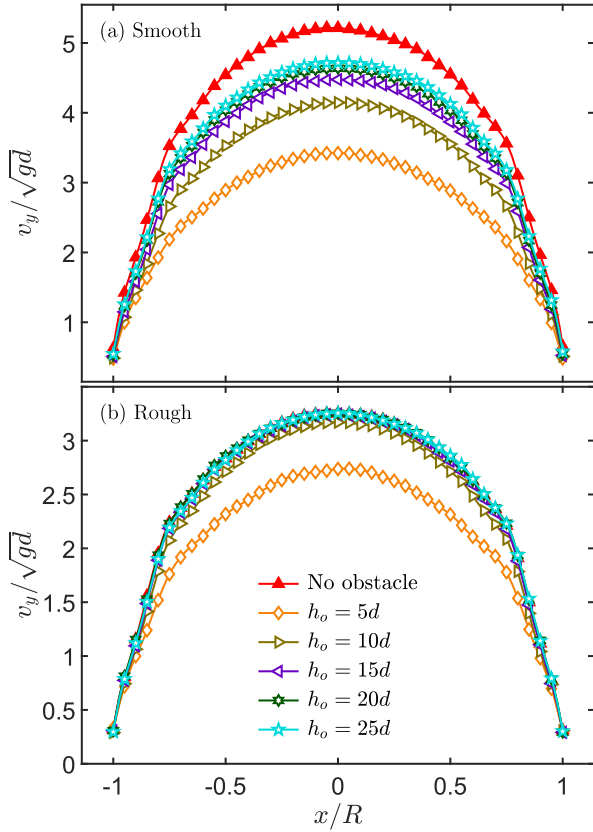


Figure 3. Vertical velocity profiles at the exit for the smooth- and rough-wall systems in the absence and presence of an obstacle located at h_o , where $R = D/2$. Labels for both plots are given in (b).

profiles of the vertical velocity and solid fraction at the aperture, which we do so next.

3.2 Velocity and solid fraction

The profiles of the vertical velocity v_y at the outlet are displayed in Figs. 3(a) and 3(b) for the smooth- and rough-wall systems, respectively, for varying obstacle locations. It is expected that the profiles are symmetric about the outlet center and grains descend faster in the smooth-wall case. For the rough case, the profiles overlap with their no-obstacle counterpart as the obstacle rises above a threshold height. However, such a behaviour is not displayed by the smooth-wall system.

In contrast to velocity, the profiles of solid fraction depict a different story in Figs. 4(a) and 4(b). Interestingly, in comparison with the no-obstacle case, the density of grains passing through the aperture does not change for higher obstacle placements ($h_o > 10d$) for both the smooth and rough walls. It is, nonetheless, important to note that the solid fraction is higher for the smooth-wall case than the rough-wall scenario for all obstacle locations. This observation aligns with the study reporting a denser packing of frictionless particles than frictional ones [14].

Similarly to what we did earlier for the flow rate, we now estimate the reduction in velocity and density of grains at the exit in the presence of an obstacle, taking the

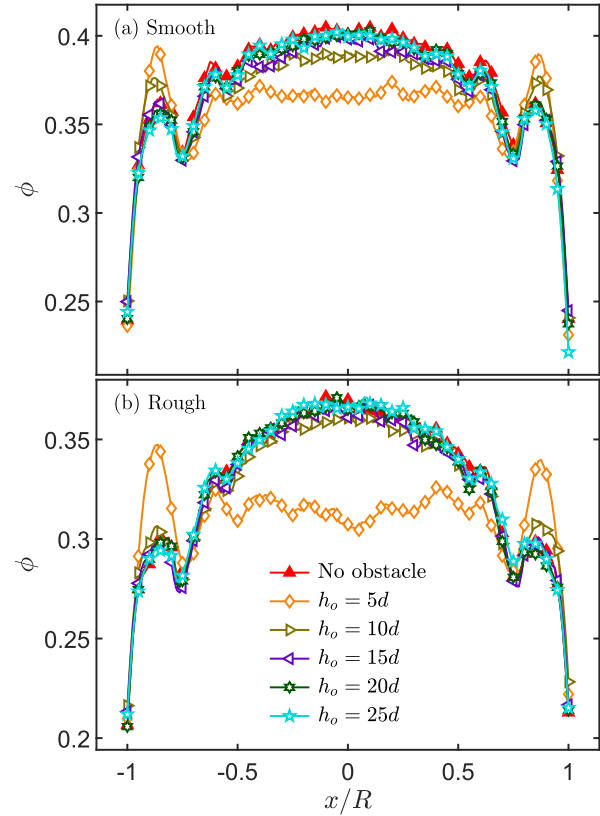


Figure 4. Solid fraction profiles at the outlet the smooth- and rough-wall silos. Here, $R = D/2$. Legend for both plots is provided given in (b).

no-obstacle case as a reference. To this end, without loss of generality, we consider the velocity and density at the outlet center and scale them by their respective values for the no-obstacle case. The variation of scaled central velocity and density with h_o is shown, respectively, in Figs. 5(a) and 5(b). The velocity exhibits a trend quite similar to the mass flow rate; that is, the reduction in velocity is higher for the smooth-wall system [cf. Fig. 2(b)]. On the other side, the change in density is less than the rough-wall case. Looking collectively, we note that the velocity is affected the most with the presence of an obstacle. The effects are prominently reflected for the smooth-wall system.

4 Summary

This study examines the effect of an obstacle on granular kinematics in quasi-two-dimensional silos with smooth and rough walls, along the thickness, using computations based on the discrete element method. The results show that the mass flow rate increases with obstacle height, reaching the no-obstacle value for the rough-wall system. However, the smooth-wall silo does not attain the flow rate corresponding to the no-obstacle scenario for the obstacle placements considered in this study. The vertical velocity follows a similar trend, whereas the solid fraction exhibits contrasting features, necessitating further investigation to reconcile the granular dynamics manifested in the smooth- and rough-wall systems.

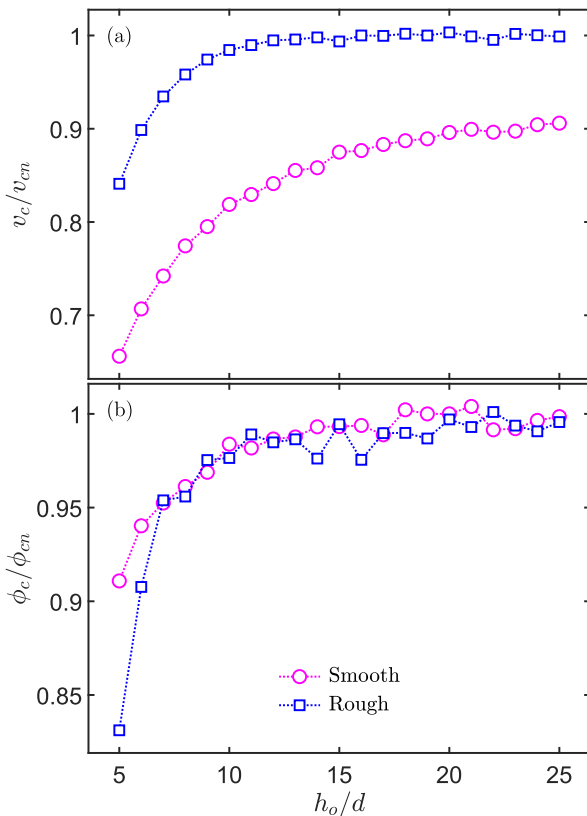


Figure 5. Variation of the scaled central velocity and solid fraction with h_o . Here, v_c and v_{cn} represent the vertical velocity at the outlet center in silos with and without obstacles, respectively. Similarly, the solid fraction is denoted by ϕ_c and ϕ_{cn} .

References

- [1] K. Saleh, S. Golshan, R. Zarghami, A review on gravity flow of free-flowing granular solids in silos—basics and practical aspects, *Chemical Engineering Science* **192**, 1011 (2018). <https://doi.org/10.1016/j.ces.2018.08.028>
- [2] I. Zuriguel, A. Janda, A. Garcimartín, C. Lozano, R. Arévalo, D. Maza, Silo clogging reduction by the presence of an obstacle, *Physical Review Letters* **107**, 278001 (2011). <https://doi.org/10.1103/PhysRevLett.107.278001>
- [3] C. Lozano, A. Janda, A. Garcimartin, D. Maza, I. Zuriguel, Flow and clogging in a silo with an obstacle above the orifice, *Physical Review E* **86**, 031306 (2012). <https://doi.org/10.1103/PhysRevE.86.031306>
- [4] A. B. Harada, E. Thackray, K. N. Nordstrom, Silo flow and clogging in the presence of an obstacle, *Physical Review Fluids* **7**, 054301 (2022). <https://doi.org/10.1103/PhysRevFluids.7.054301>
- [5] D. Zhang, X. Yang, H. Guo, Z. Tian, X. Liu, Why the presence of insert above the outlet can enhance silo discharge: a tentative answer, *Powder Technology* **421**, 118384 (2023). <https://doi.org/10.1016/j.powtec.2023.118384>
- [6] F. Alonso-Marroquin, S. I. Azeezullah, S. A. Galindo-Torres, L. M. Olsen-Kettle, Bottlenecks in granular flow: when does an obstacle increase the flow rate in an hour-glass?, *Physical Review E* **85**, 020301 (2012). <https://doi.org/10.1103/PhysRevE.85.020301>
- [7] K. Endo, K. A. Reddy, H. Katsuragi, Obstacle-shape effect in a two-dimensional granular silo flow field, *Physical Review Fluids* **2**, 094302 (2017). <https://doi.org/10.1103/PhysRevFluids.2.094302>
- [8] G. J. J. Gao, F. L. Yang, M. C. Holcomb, J. Blawdziewicz, Enhanced flow rate by the concentration mechanism of tetris particles when discharged from a hopper with an obstacle, *Physical Review E* **103**, 062904 (2021). <https://doi.org/10.1103/PhysRevE.103.062904>
- [9] D. Gella, D. Yanagisawa, R. Caitano, M. V. Ferreyra, I. Zuriguel, On the dual effect of obstacles in preventing silo clogging in 2D, *Communications Physics* **5** (2022). <https://doi.org/10.1038/s42005-021-00756-4>
- [10] R. Caitano, A. Garcimartín, I. Zuriguel, Anchoring effect of an obstacle in the silo unclogging process, *Physical Review Letters* **131**, 098201 (2023). <https://doi.org/10.1103/PhysRevLett.131.098201>
- [11] P. A. Cundall, O. D. L. Strack, A discrete numerical model for granular assemblies, *Géotechnique* **29**, 47 (1979). <https://doi.org/10.1680/geot.1979.29.1.47>
- [12] <https://www.lammps.org/>
- [13] L. E. Silbert, D. Ertaş, G. S. Grest, T. C. Halsey, D. Levine, S. J. Plimpton, Granular flow down an inclined plane: Bagnold scaling and rheology, *Physical Review E* **64**, 051302 (2001). <https://doi.org/10.1103/PhysRevE.64.051302>
- [14] L. E. Silbert, D. Ertaş, G. S. Grest, T. C. Halsey, D. Levine, Geometry of frictionless and frictional sphere packings, *Physical Review E* **65**, 031304 (2002). <https://doi.org/10.1103/PhysRevE.65.031304>